INTERNATIONAL JOURNAL FOR NUMERICAL METHODS IN FLUIDS
Int. J. Numer. Meth. Fluids 2007; **55**:1091–1120
Published online 27 June 2007 in Wiley InterScience (www.interscience.wiley.com). DOI: 10.1002/fld.1545

On the effects of a compressible viscous lubricant on the load-bearing capacity of a journal bearing

P. C. Bollada and T. N. Phillips*, †

School of Mathematics, Cardiff University, Senghennydd Road, Cardiff CF24 4AG, U.K.

SUMMARY

A compressible viscous isothermal model is presented for studying journal-bearing lubrication. The viscosity in the model thickens with increasing density. The governing equations are written in terms of velocity, the natural logarithm of the density and the kinematic extra-stress tensor. A semi-Làgrangian treatment of the material derivatives is combined with a spectral element discretization in space. The roles of the speed of sound and the eccentricity ratio on the load-bearing capacity of the journal bearing are investigated. Compressibility is shown to enhance the load-bearing capacity and this effect is amplified as the eccentricity ratio approaches unity. It is shown that for speeds of sound in the region of those of multigrade oils, the dominant component of the force on the journal acts along the line joining the centres of the bearing and journal and in the direction away from the narrow gap. Copyright © 2007 John Wiley & Sons, Ltd.

Received 1 December 2006; Revised 9 May 2007; Accepted 12 May 2007

KEY WORDS: *journal-bearing*; compressible fluid; spectral element method; semi-Lagrangian discretization; lubrication

1. INTRODUCTION

Lubrication in journal bearings is of considerable interest and importance within the automotive industry. The ability to predict the performance of a lubricant within this engineering setting is important to the manufacture and processing of oils that have the capacity to reduce friction and wear, and hence ensure that engine components run smoothly and have an adequate longevity.

In this paper, we consider hydrodynamic lubrication. In this lubrication regime, the elastic deformation of the journal and bearing surfaces are assumed to be insignificant. Our understanding

*Correspondence to: T. N. Phillips, School of Mathematics, Cardiff University, Senghennydd Road, Cardiff CF24 4AG, U.K.
†E-mail: phillipstn@cf.ac.uk

Contract/grant sponsor: E.P.S.R.C

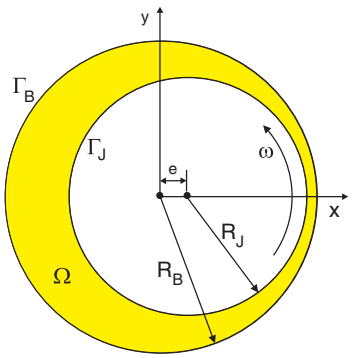

Figure 1. Schematic picture of a journal bearing with the difference in radius exaggerated for clarity.

of hydrodynamic lubrication dates back to the pioneering experiments of Tower [1], in which the existence of a film was detected from measurements of pressure within a lubricant. The same conclusion was reached by Petrov [2–5] using friction measurements. This work was rapidly followed by some theoretical work of Reynolds [6], who introduced what is known as the lubrication approximation. This approximation enables a second-order differential equation for the pressure in the narrow, converging gap between the journal and the bearing to be derived.

This facilitates the calculation of the load on the journal. In some situations, an analytical expression for the load and torque on the journal can be derived. This shows that the pressure enables a load to be transferred between the surfaces with extremely low friction, since the surfaces are separated by a fluid film. A positive pressure is generated by the convergence of the journal and bearing surfaces, the relative motion between the surfaces and the viscosity of the lubricant. The existence of the positive pressure serves to support a normal applied load.

In an order of magnitude analysis of Navier–Stokes equations, Hamrock [7] shows that the inertial term is of order h/l where h and l are characteristic lengths associated with the radial and azimuthal directions, respectively, and can be taken to be the average gap between the journal and bearing, and the radius of the journal. On the other hand, the pressure gradient and viscous terms are of order 1. By neglecting terms of order h/l (the inertial term) in the Navier–Stokes equations (Stokes flow) we note that, for any given solution $(\mathbf{u}, p)$ then $(-\mathbf{u}, -p)$ is also a solution. Using this together with the symmetry of the geometry (see Figure 1) infers that the pressure p is antisymmetric about the small gap. Thus, we expect that the force imparted along the line joining the journal and bearing centres will be much less significant than the force normal to this line. In this paper, we show that the presence of compressibility changes this picture for high eccentricity ratios.

In the previous work on the journal-bearing problem [8–11], it was assumed that the lubricant was incompressible. The motivation behind this study is to broaden the modelling assumption to include compressibility. Compressibility may play an important role in journal-bearing lubrication for a number of reasons.

First, the observation has been made that cavitation has a beneficial effect on the dynamics of a physically engineered journal bearing in that it can stabilize the motion of the journal. There are two main types of cavitation: gaseous and vapour. Gaseous cavitation occurs when the pressure of the lubricant falls below the ambient pressure level and this subambient region is replaced by

DOI: 10.1002/fld

air. Vapour cavitation occurs when the lubricant reaches such low pressures that it 'boils' and air that was previously in solution appears as vapour. The pressure levels required for vapour cavitation are generally much lower than for gaseous cavitation. This paper is concerned with a 2D configuration and in this geometry there is no mechanism for the occurrence of gaseous cavitation since there are no holes or openings for air to enter since it is a confined flow. For vapour cavitation, the assumption that fluid particles remain fluid particles is not valid since the gas appears out of solution from the oil. Therefore, cavitation can only realistically be modelled by invoking compressibility.

Secondly, the study of flow phenomena associated with compressible fluids is important in order to understand fully many other industrial processes apart from journal-bearing lubrication. In the realm of non-Newtonian and viscoelastic fluids, for example, we cite injection moulding and high-speed extrusion as situations in which pressure and flow rate may become large. In these situations, compressibility effects may become very important. As noted by Belblidia *et al*. [12], there are a number of advantages in working with compressible flow, e.g. the compatibility of discrete function spaces.

Thirdly, a more natural model for viscosity in journal bearings should incorporate an element of density thickening rather than the pressure thickening model presented in Gwynllyw and Phillips [13]. The model presented here sets viscosity to be proportional to density which in turn is linearly related to pressure. Thus, *kinematic* viscosity is assumed to be constant and allows significant simplification in the momentum equations. However, such a simplification needs to treated with caution. For comparison, isothermal examples of pressure-dependent viscosity, are the Barus equation [14]

$$\eta = \eta_0 \exp(\alpha(p - p_0))$$

which is thought to be effective at low pressure and the Roelands equation [15]

$$\eta = \eta_0 \exp\{(\ln \eta_0 + a)[(1 + b(p - p_0))^z - 1]\}$$

where the index $z = \alpha/[b(\ln \eta_0 + a)]$, and typical values for the constants (in S.I. units) are, $\alpha = 2.1 \times 10^{-8}$, $a = 9.67$, $b = 5.1 \times 10^{-9}$. Taking the Barus relation as an example, we find using a linear equation of state for pressure $p = c^2\rho$ that $\alpha = 2.1 \times 10^{-8}\,\mathrm{m^2/N}$, $\rho_0 = 400\,\mathrm{kg/m^3}$ and $c = 1500\,\mathrm{m/s}$ gives a change in viscosity of 20% for a 1% change in density. Since we find changes of pressure of up to 10% in our simulation this clearly gives different values of stress when compared with the Barus model and some results (e.g. the torque on the journal) can only be viewed qualitatively. Having said this, however, it is computationally expedient to use the constant kinematic viscosity to keep the equations linear keeping in mind that the main thrust of this paper is an exploration of the role of *compressibility* on the load-bearing capacity. Refinements to the model including the viscosity relations given above, temperature thinning, elasticity and realistic equations of state will be explored in a subsequent paper. Initial results suggest, for example, that a Barus law exaggerates the load-bearing capacity and temperature and shear thinning reduces the effect.

The compressibility of a fluid is intimately connected with the speed of sound, c. In this initial model, this can be kept constant but at a later stage it may be given as a function of density (or pressure) to reflect the differences in the speed of sound of c in the liquid and gas phases. In this first exposition of a compressible model in the journal-bearing problem, we explore the loads on

DOI: 10.1002/fld

the journal for a series of values of sound speed c, journal radius and eccentricity. A particular feature of the model is its similarity to Navier–Stokes equations with constant dynamic viscosity replaced by that of constant kinematic viscosity plus an extra term associated with compressibility essential for a general isotropic fluid [16]. By taking increasingly large values of c the model presented gives an alternative way of simulating *incompressible* Newtonian fluids avoiding the well-known problems associated with incompressibility constraint $\nabla \cdot \mathbf{u} = 0$.

A semi-Lagrangian scheme for treating the material derivative is employed within the numerical scheme. The method takes full advantage of the continuous approximations generated by the spectral element method, which can be easily evaluated away from the grid points. The relative simplicity of the model ensures that computation times are rapid and allows a high-order spectral approximation to be used. Converged approximations are obtained either by increasing the order of polynomial approximation or by increasing the number of spectral elements—even when the journal is highly eccentric and its radius differs significantly from that of the bearing.

The structure of the paper is as follows. In Section 2, the governing equations are presented for the compressible isothermal viscous fluid and the speed of sound is discussed in the context of the fluid model. In Section 3, the discretization of the material derivative is discussed and the new geometric method presented. In Section 4, the weak formulation and spatial discretization process is presented. In Section 5, some numerical results are presented showing the influence of the speed of sound and the eccentricity ratio on the load-bearing capacity of the journal bearing. A study of numerical convergence is also provided. Concluding remarks and a discussion of further research activities in this area are given in Section 6.

2. GOVERNING EQUATIONS FOR A COMPRESSIBLE VISCOUS FLUID

The lubricant is modelled as a compressible viscous fluid. Using constant kinematic viscosity rather than constant dynamic viscosity, it is possible to ensure that most of the non-inertial terms in the governing equations remain linear. The nonlinear stress term is negligible for near incompressible flow so by choosing a large value for c, for example, one can obtain predictions that are close to those for a Newtonian fluid.

2.1. Conservation equations

The conservation of momentum, or equation of motion, for a fluid is

$$\rho \frac{\mathrm{D}\mathbf{u}}{\mathrm{D}t} = -\nabla p + \nabla \cdot \mathbf{S} \tag{1}$$

where ρ is the density, $\mathbf{u}$ is the velocity, p is the pressure, and $\mathbf{S}$ is the extra-stress tensor. The extra-stress tensor for a compressible viscous fluid is given by

$$\mathbf{S} = \eta_1(\nabla \mathbf{u} + \nabla \mathbf{u}^{\mathrm{T}}) + \eta_2(\nabla \cdot \mathbf{u})\mathbf{I} \tag{2}$$

where η_1 is the dynamic coefficient of viscosity (shear) and η_2 is the second coefficient of viscosity (dilatational). The quantity $\frac{2}{3}\eta_1 + \eta_2$ is known as the bulk viscosity [16]. The bulk viscosity is relevant only in situations where the density is changing. Thus, it plays a role in attenuating sound waves in fluids and may be estimated from the magnitude of the attenuation.

DOI: 10.1002/fld

The conservation of mass, or equation of continuity, is written as

$$\frac{\mathrm{D}\rho}{\mathrm{D}t} = -\rho\nabla\cdot\mathbf{u} \tag{3}$$

The second viscosity coefficient is typically set to $\eta_2 = -\frac{2}{3}\eta_1$, which means that the bulk viscosity is zero and ensures that $\mathrm{tr}(\mathbf{S}) = 0$. This is known as Stokes' hypothesis. However, the validity of this hypothesis is one of the unanswered questions in fluid mechanics. Gad el Hak [16] argues that the hypothesis does not hold, in general, and suggests that the value of the second coefficient of viscosity should be positive with measurable effects in shock wave situations. On the other hand, Phan-Thien [17] states that the $\eta_2(\nabla\cdot\mathbf{u})\,\mathbf{I}$ term *can be absorbed into the pressure term*. It appears to be the case that a physical measurement of pressure corresponds to a measurement of $-\frac{1}{3}\mathrm{tr}(\boldsymbol{\sigma})$ (where $\boldsymbol{\sigma} = -p\mathbf{I} + \mathbf{S}$ is the total stress), which for zero bulk viscosity corresponds to the variable p. Since this paper is largely concerned with the force on a fixed rotating journal, the relevance of these questions, as they pertain to journal bearings, can be largely addressed by finding the resultant forces for a range of values of bulk viscosities.

2.2. Equation of state and kinematic stress

For isothermal flow, we assume the existence of an equation of state

$$p = p(\rho)$$

so that

$$\nabla p = \frac{\mathrm{d}p}{\mathrm{d}\rho}\nabla\rho$$

We assume viscosity is linearly dependent on density

$$\eta_1 = \mu\rho, \quad \eta_2 = \nu\rho$$

for some constant kinematic viscosity μ and $\nu(=-\frac{2}{3}\mu)$. Thus, we can rewrite (1) and (3) as

$$\frac{\mathrm{D}\mathbf{u}}{\mathrm{D}t} = -\frac{\mathrm{d}p}{\mathrm{d}\rho}\nabla q + \nabla\cdot\mathbf{T} + \nabla q\cdot\mathbf{T} \tag{4}$$

and

$$\frac{\mathrm{D}q}{\mathrm{D}t} = -\nabla\cdot\mathbf{u} \tag{5}$$

where the kinematic extra stress is defined

$$\mathbf{T} \equiv \mu(\nabla\mathbf{u} + \nabla\mathbf{u}^{\mathrm{T}}) + \nu(\nabla\cdot\mathbf{u})\mathbf{I} \tag{6}$$

and we define the log density

$$q \equiv \ln\rho \tag{7}$$

DOI: 10.1002/fld

Choosing an equation of state, $p = c^2\rho$, for constant speed of sound c (see Section 2.3) gives

$$\frac{\mathrm{D}\mathbf{u}}{\mathrm{D}t} = -c^2\nabla q + \nabla\cdot\mathbf{T} + \nabla q\cdot\mathbf{T} \tag{8}$$

We have chosen this equation of state since the variation of density with pressure is approximately linear at low pressures. At high pressures, the rate of increase is found to be sublinear.

An alternative equation of state that has been used in polymer processing is the so-called Tait equation:

$$p + B = B\left(\frac{\rho}{\rho_0}\right)^m \tag{9}$$

where ρ_0 is the density of the fluid extrapolated to zero pressure. In the Tait equation, B is a weak function of entropy and m is a non-dimensional power-law index, not to be confused with the ratio of specific heats. However, in practice B is taken to be constant and is used to represent a non-dimensional shift for the pressure. Although this equation is normally attributed to Tait, it bears little resemblance to the equation originally proposed by Tait and used by him to fit data for sea water. In fact, Equation (9) is a modification of Tait's original equation suggested by Kirkwood and Bethe [18, 19]. The speed of sound in the modified Tait equation of state is given by

$$c^2 = \left(\frac{mB}{\rho_0}\right)\left(\frac{\rho}{\rho_0}\right)^{m-1} = \frac{mB}{\rho_0^m}\mathrm{e}^{(m-1)q} \tag{10}$$

Another density–pressure relation widely used in elastohydrodynamic lubrication is [15, 20]

$$\rho = \rho_0[1 + ap/(1 + bp)]$$

We can rewrite this as

$$p = c_0^2\frac{\rho - \rho_0}{1 + C(1 - \rho/\rho_0)}$$

where $c_0^2 = 1/(\rho_0 a)$ and $C = bc_0^2\rho_0$. For typical values of $C \approx 1.5$ and a comparison with the Tait equation suggests that with $m \approx 4$ the models agree well for $\rho = \rho_0 \pm 10\%$.

2.3. A note on the speed of sound

Consider the measurement of the speed of sound in a stationary bath of fluid. Given the equations of continuity and momentum and, following the approach outlined in the book of Billingham and King [21], we perturb the system: $p = p_0 + \tilde{p}$, $\rho = \rho_0 + \tilde{\rho}$ and $\mathbf{u} = \tilde{\mathbf{u}}$. The equations in the perturbed quantities are then

$$\frac{1}{\rho_0}\frac{\partial\tilde{\rho}}{\partial t} = -\nabla\cdot\tilde{\mathbf{u}} \tag{11}$$

and

$$\frac{\partial\tilde{\mathbf{u}}}{\partial t} = -\frac{1}{\rho_0}\nabla\tilde{p} + \frac{1}{\rho_0}[\eta_1\nabla^2\tilde{\mathbf{u}} + (\eta_1 + \eta_2)\nabla(\nabla\cdot\tilde{\mathbf{u}})] \tag{12}$$

DOI: 10.1002/fld

Taking the divergence of (12) (assuming $\nabla\eta_1$ and $\nabla\eta_2$ are both negligible) gives

$$\frac{\partial \nabla\cdot\tilde{\mathbf{u}}}{\partial t} = -\frac{1}{\rho_0}\frac{\partial^2\tilde{\rho}}{\partial t^2} = -\frac{1}{\rho_0}\nabla^2\tilde{p} + \frac{1}{\rho_0}(2\eta_1+\eta_2)\nabla^2(\nabla\cdot\tilde{\mathbf{u}})$$

implying that $\tilde{\rho}$ satisfies the wave equation

$$\frac{\partial^2\tilde{\rho}}{\partial t^2} = \nabla^2[\tilde{p} - (2\eta_1+\eta_2)(\nabla\cdot\tilde{\mathbf{u}})] \tag{13}$$

Now, $p = c^2(\rho+\rho_0)$ implies $\tilde{p} = c^2\tilde{\rho}$ and so with $\eta_2 = -\frac{2}{3}\eta_1$

$$\frac{1}{c^2}\frac{\partial^2\tilde{p}}{\partial t^2} = \nabla^2\tilde{p} - \frac{4}{3}\eta_1\nabla^2(\nabla\cdot\tilde{\mathbf{u}}) \tag{14}$$

Finally, using (11) to eliminate $\nabla\cdot\tilde{\mathbf{u}}$ gives

$$\ddot{p} = \nabla^2\left[c^2\tilde{p} + \frac{4\mu}{3}\dot{p}\right]$$

where $\dot{p} \equiv \partial\tilde{p}/\partial t$ and $\mu \equiv \eta/\rho_0$. This equation has an attenuated wave solution with wave speed, a, given by

$$a \equiv \sqrt{c^2 - \left(\frac{\alpha k}{2}\right)^2} \tag{15}$$

and attenuation $\exp(-\frac{1}{2}\alpha k^2)$ where k is the wave number and $\alpha \equiv \frac{4}{3}\mu$. For general μ, ν the result is $\alpha = 2\mu + \nu$. For a value of $\mu = 1.25\times10^{-5}\,\mathrm{m^2/s}$ used in [13] and sound speed $c > 340\,\mathrm{m/s}$ then clearly $c \approx a$ with little attenuation for frequencies below ultra sonic. However, for higher frequencies it may be possible to measure α and so verify $\nu = -\frac{2}{3}\mu$ with μ measured indirectly by such a method [16].

3. THE STATICALLY LOADED JOURNAL-BEARING PROBLEM

Consider the 2D geometry shown schematically in Figure 1. The journal of radius R_J rotates with a predetermined constant angular velocity ω about its own centre. The journal's motion is lubricated by a fluid lubricant contained within a stationary bearing of radius R_B. Both the journal and the bearing are assumed to be of infinite extent in the axial z-direction. The time-dependent eccentricity of the system is denoted by e, with the eccentricity ratio defined by $\varepsilon = e/(R_\mathrm{B} - R_\mathrm{J})$, $0 \leqslant \varepsilon \leqslant 1$. Therefore, when $\varepsilon = 1$ the journal is in contact with the bearing and when $\varepsilon = 0$ the journal and bearing are concentric.

The lubricant satisfies the governing equations (5), (6) and (8) which are solved subject to specified boundary and initial conditions. These are, respectively,

$$\mathbf{u}(\mathbf{x},t) = \mathbf{V}(t) \quad \text{with } \mathbf{x}\in\Gamma_\mathrm{J}, \quad \mathbf{u}(\mathbf{x},t) = \mathbf{0} \quad \text{with } \mathbf{x}\in\Gamma_\mathrm{B} \tag{16}$$

$$\mathbf{u}(\mathbf{x},t=0) = \mathbf{0} \tag{17}$$

where Γ_J and Γ_B denote the boundaries of the journal and bearing, respectively.

DOI: 10.1002/fld

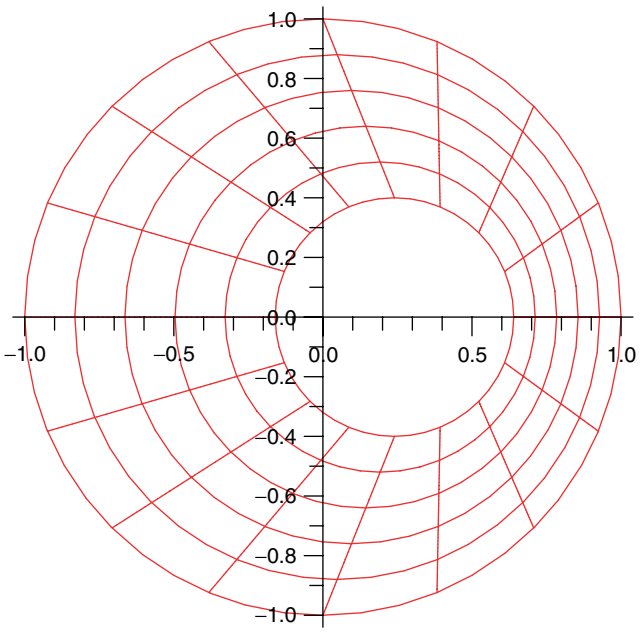

Figure 2. A coordinate system for the journal bearing. This coordinate system has the feature that constant r describes a circle and radial lines meet at the point $(e, 0)$.

We consider the following coordinate system in the journal-bearing configuration (see Figure 2):

$$x = r\cos\theta + \varepsilon(1 - r) \tag{18}$$

$$y = r\sin\theta \tag{19}$$

for $r \in [R, 1]$ and $\theta \in [0, 2\pi]$, where the radial distance has been scaled by R_B. The eccentricity ratio, in terms of the scaled radius, is now defined by

$$\varepsilon = \frac{e}{1 - R}$$

The derivatives associated with the transformation are related through

$$\begin{bmatrix} \dfrac{\partial}{\partial r} \\ \dfrac{\partial}{\partial \theta} \end{bmatrix} = \begin{bmatrix} \cos\theta - \varepsilon & \sin\theta \\ -r\sin\theta & r\cos\theta \end{bmatrix} \begin{bmatrix} \dfrac{\partial}{\partial x} \\ \dfrac{\partial}{\partial y} \end{bmatrix}$$

so that

$$\begin{bmatrix} \dfrac{\partial}{\partial x} \\ \dfrac{\partial}{\partial y} \end{bmatrix} = \begin{bmatrix} r\cos\theta/J_1 & -(\sin\theta)/J_1 \\ r\sin\theta/J_1 & (\cos\theta - \varepsilon)/J_1 \end{bmatrix} \begin{bmatrix} \dfrac{\partial}{\partial r} \\ \dfrac{\partial}{\partial \theta} \end{bmatrix}$$

DOI: 10.1002/fld

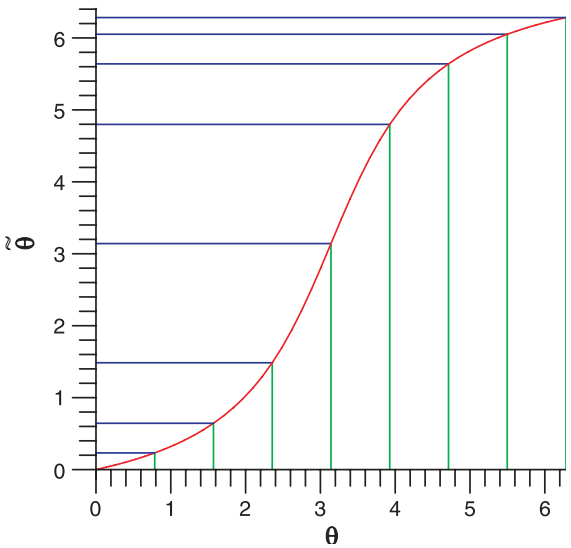

Figure 3. Pictorial representation of the stretching function $\tilde{\theta}$.

where $J_1 \equiv r(1 - \varepsilon \cos\theta)$. The above mapping can be refined by including a stretching function, $\tilde{\theta} : [0, 2\pi] \to [0, 2\pi]$, to aid with mesh refinement in the region of the narrow gap, corresponding to $\theta = 0$, where the large pressure gradients occur. Essentially, this can be achieved by using some form of the inverse tangent function, viz.

$$\tilde{\theta}(\theta) = \frac{\pi(1 + \tan^{-1}[a(\theta - \pi)])}{\tan^{-1}(a\pi)}$$

This mapping is illustrated in Figure 3. It has an explicit inverse representation $\tilde{\theta}^{-1} : [0, 2\pi] \to [0, 2\pi]$ (required by the semi-Lagrangian discretization) given by

$$\tilde{\theta}^{-1}(\theta) = \pi + \frac{1}{a} \tan^{-1}(\tan^{-1}(a\pi)(\theta - \pi)/\pi)$$

4. LAGRANGIAN DESCRIPTION OF THE MATERIAL DERIVATIVE

The discretization of the governing equations for an incompressible fluid in an Eulerian framework results in a system of equations that is nonlinear and non-symmetric. To overcome this problem, the convection terms in the equations are generally treated explicitly. This avoids the need to perform a linearization of the equations using Newton's method, for example, and to solve the resulting linear systems of equations using iterative techniques such as GMRES and its variants. However, the use of an explicit discretization of the convection term results in a restriction on the size of time step that can be used for stability reasons. The principal computational expense is then associated with the inverse of a generalized Stokes operator.

DOI: 10.1002/fld

An alternative to the use of explicit Adams–Bashforth methods for the convection term is to use a backward differentiation (BDF) method combined with an extrapolation of the nonlinear convection terms. Karniadakis *et al*. [22] proposed a third-order BDF combined with a third-order extrapolation scheme to evaluate the convection term at the new time level. The resulting scheme is globally third-order accurate and is devoid of any time-splitting error.

Another class of methods that is used in the numerical simulation of the Navier–Stokes equations is based on the use of fractional steps in which the treatment of the nonlinear terms, incompressibility and the viscous terms are decoupled. The second step, which forces the velocity field to be incompressible, results in the construction of a Poisson problem for the pressure for which consistent boundary conditions need to be imposed. A detailed account of transient schemes used in conjunction with spectral methods can be found in the monograph of Deville *et al*. [23].

In this section, the discretization of the material derivatives in the conservation equations is described. A Lagrangian rather than an Eulerian description of the material derivative is preferred. However, in order to avoid computational problems associated with excessive particle movement such as the distortion of the spectral element mesh, a semi-Lagrangian approach is adopted. In our implementation of this approach, the spectral element mesh remains fixed and the material derivative is discretized in a Lagrangian sense over a single time step. There are two material derivatives in the governing equations for a compressible viscous fluid and these account for all but one of the nonlinear terms in these equations. The natural framework within which to discretize the material derivative terms is the Lagrangian framework and it is this which we describe here.

Consider the momentum equation written in the form

$$\frac{\mathrm{D}\mathbf{u}}{\mathrm{D}t} = \mathbf{f}(\mathbf{u}) \tag{20}$$

where $\mathbf{f}$ is an implicit vector function of $\mathbf{u}$ defined by

$$\mathbf{f}(\mathbf{u}) = -c^2 \nabla q + \nabla \cdot \mathbf{T} + \nabla q \cdot \mathbf{T} \tag{21}$$

The implicitness arises from definition (6) of $\mathbf{T}$ as a function of $\mathbf{u}$ and the observation that q is a function of $\mathbf{u}$ *via* continuity equation (5). Therefore, $\mathbf{f}$ is an implicit function of $\mathbf{u}$ and position only. We may also write momentum equation (20) in the form

$$\frac{\partial \mathbf{u}}{\partial t} + \mathbf{u} \cdot \nabla \mathbf{u} = \mathbf{f}(\mathbf{u})$$

The temporal discretization of this equation using an implicit backward-Euler scheme at given points $\mathbf{x}$ results in the following nonlinear equation for $\mathbf{u}^{n+1}$:

$$\frac{\mathbf{u}^{n+1}(\mathbf{x}) - \mathbf{u}^{n}(\mathbf{x})}{\Delta t} + \mathbf{u}^{n+1}(\mathbf{x}) \cdot \nabla \mathbf{u}^{n+1}(\mathbf{x}) = \mathbf{f}(\mathbf{u}^{n+1}) \tag{22}$$

where all terms are evaluated at the same spatial point, $\mathbf{x}$. This is the essence of an Eulerian description of the problem. Consider a particle located at position $\mathbf{x} = \mathbf{x}^{n+1}$ at time $t = t^{n+1}$. Then substituting $\mathbf{x} = \mathbf{x}^{n+1}$ in (22) we have

$$\frac{\mathbf{u}^{n+1}(\mathbf{x}^{n+1}) - \mathbf{u}^{n}(\mathbf{x}^{n+1})}{\Delta t} + \mathbf{u}^{n+1}(\mathbf{x}^{n+1}) \cdot \nabla \mathbf{u}^{n+1}(\mathbf{x}^{n+1}) = \mathbf{f}(\mathbf{u}^{n+1}(\mathbf{x}^{n+1})) \tag{23}$$

DOI: 10.1002/fld

We note that the particles at the point $\mathbf{x}=\mathbf{x}^{n+1}$ at times $t=t^n$ and $t=t^{n+1}$ are different, in general. This is the cause of the nonlinearity. Suppose that the particle located at the position $\mathbf{x}^{n+1}$ at time $t=t^{n+1}$ was at the position $\mathbf{x}^n$ at $t=t^n$, then we may write the time discretization of the material derivative in Lagrangian form

$$\frac{\mathbf{u}^{n+1}(\mathbf{x}^{n+1})-\mathbf{u}^n(\mathbf{x}^n)}{\Delta t}=\mathbf{f}(\mathbf{u}^{n+1}(\mathbf{x}^{n+1})) \tag{24}$$

The Lagrangian derivative is a derivative along particle trajectories. The nonlinearity on the left-hand side of (23) is now removed from the discretization. However, now the problem is how to determine $\mathbf{x}^n$ and to evaluate $\mathbf{u}^n(\mathbf{x}^n)$ using some form of interpolation since, in general, $\mathbf{x}^n$ will not be located at a grid point. One option is to use the Taylor series for position

$$\begin{aligned}\mathbf{x}^n&=\mathbf{x}^{n+1}-\Delta t\mathbf{u}^{n+1}(\mathbf{x}^{n+1})+\frac{1}{2}\Delta t^2\frac{\mathrm{D}}{\mathrm{D}t}\mathbf{u}^{n+1}(\mathbf{x}^{n+1})+O(\Delta t^3)\\&=\mathbf{x}^{n+1}-\Delta t\mathbf{u}^{n+1}(\mathbf{x}^{n+1})+\frac{1}{2}\Delta t^2\mathbf{f}(\mathbf{u}^{n+1}(\mathbf{x}^{n+1}))+O(\Delta t^3)\end{aligned} \tag{25}$$

i.e. we calculate the previous position of the particle from a knowledge of its current position, velocity and acceleration. Now using Taylor expansion for vector fields $\mathbf{v}$ about a point $\mathbf{x}$ in space:

$$\mathbf{v}(\mathbf{x}+\delta\mathbf{x})=\mathbf{v}(\mathbf{x})+\nabla_{\delta\mathbf{x}}\mathbf{v}(\mathbf{x})+\tfrac{1}{2}\nabla_{\delta\mathbf{x}}\nabla_{\delta\mathbf{x}}\mathbf{v}(\mathbf{x})+O(|\delta\mathbf{x}|^3)$$

where $\delta\mathbf{x}$ is assumed to be a small displacement and $\nabla_{\delta\mathbf{x}}\mathbf{v}\equiv\delta\mathbf{x}\cdot\nabla\mathbf{v}$. To first order this gives the scheme

$$\frac{\mathbf{u}^{n+1}-\mathbf{u}^n}{\Delta t}+\mathbf{u}^{n+1}\cdot\nabla\mathbf{u}^n=\mathbf{f}^{n+1}(\mathbf{u}^{n+1}) \tag{26}$$

There are two disadvantages with (26). Unlike (22), the scheme is not symmetric and also retains the disadvantage of altering the inertial contribution to the system at every time step lowering computational efficiency. For example, a scheme such as

$$\frac{\mathbf{u}^{n+1}-\mathbf{u}^n}{\Delta t}+\mathbf{u}^n\cdot\nabla\mathbf{u}^n=\mathbf{f}^{n+1}(\mathbf{u}^{n+1})$$

has the advantage of being both more efficient and symmetric; though having the disadvantage of being less stable in transient flow and generally requiring smaller time steps.

We now present an alternative to the forgoing using an iterative scheme. First, instead of (25), we use an alternative mid-point second-order approximation for $\mathbf{x}^n$

$$\frac{\mathbf{x}-\mathbf{x}^n}{\Delta t}=\tfrac{1}{2}(\mathbf{u}^{n+1}(\mathbf{x})+\mathbf{u}^n(\mathbf{x}^n))$$

DOI: 10.1002/fld

where we have introduced the notation $\mathbf{x} \equiv \mathbf{x}^{n+1}$. We can rewrite this equation in the form

$$\mathbf{x}^n = \mathbf{x} - \tfrac{1}{2}\Delta t[\mathbf{u}^{n+1}(\mathbf{x}) + \mathbf{u}^n(\mathbf{x}^n)] \tag{27}$$

Finally, substituting this expression for $\mathbf{x}^n$ into (24) gives

$$\frac{\mathbf{u}^{n+1}(\mathbf{x}) - \mathbf{u}^n(\mathbf{x} - \frac{1}{2}\Delta t[\mathbf{u}^{n+1}(\mathbf{x}) + \mathbf{u}^n(\mathbf{x}^n)])}{\Delta t} = \mathbf{f}(\mathbf{u}^{n+1}(\mathbf{x})) \tag{28}$$

This is a nonlinear equation for $\mathbf{u}^{n+1}(\mathbf{x})$, which can be solved using an iterative scheme at each grid point $\mathbf{x}$. Note that we do not need to solve for q in this iterative scheme since it is given explicitly in terms of $\mathbf{u}$.

Let $S = \{\mathbf{x}_j : j = 1, \ldots, L\}$ denote a set of mesh points. Then, the semi-Lagrangian procedure to determine the solution, $\mathbf{u}^{n+1}$, of (20) at each point $\mathbf{x} \in S$ at the new time level is:

1. Let $\mathbf{u}_0^{n+1}$ denote the initial approximation to $\mathbf{u}$ at time $t = t^{n+1}$. For example, a reasonable approximation is $\mathbf{u}_0^{n+1}(\mathbf{x}) = \mathbf{u}^n(\mathbf{x})$.
2. Determine an approximation, $\mathbf{x}_0^n$, to the position of the particle at time $t = t^n$ which is located at the point $\mathbf{x}$ at time $t = t^{n+1}$ by discretizing

$$\frac{\mathrm{d}\mathbf{x}}{\mathrm{d}t} = \mathbf{u}$$

along the particle path using, for example, the backward-Euler approximation

$$\mathbf{x}_0^n := \mathbf{x} - \Delta t\,\mathbf{u}_0^{n+1}(\mathbf{x})$$

3. Evaluate $\mathbf{u}^n(\mathbf{x}_0^n)$.
4. Set $m := 1$.
5. Solve the following nonlinear equation for $\mathbf{u}_m^{n+1}(\mathbf{x})$ to obtain an updated approximation for $\mathbf{u}^{n+1}(\mathbf{x})$:

$$\frac{\mathbf{u}_m^{n+1}(\mathbf{x}) - \mathbf{u}^n(\mathbf{x}_{m-1}^n)}{\Delta t} = \mathbf{f}(\mathbf{u}_m^{n+1}(\mathbf{x}))$$

6. Determine an improved approximation, $\mathbf{x}_m^n$, for the location of the particle at the previous time level using the mid-point approximation:

$$\mathbf{x}_m^n := \mathbf{x} - \frac{\Delta t}{2}(\mathbf{u}_m^{n+1}(\mathbf{x}) + \mathbf{u}^n(\mathbf{x}_{m-1}^n))$$

7. Evaluate $\mathbf{u}^n(\mathbf{x}_m^n)$.
8. If

$$\max_{\mathbf{x} \in S} |\mathbf{u}^n(\mathbf{x}_m^n) - \mathbf{u}^n(\mathbf{x}_{m-1}^n)| > \delta$$

where δ is some prescribed tolerance, then set $m := m + 1$ and go to step 5.

DOI: 10.1002/fld

10. If

$$\max_{\mathbf{x}\in S} |\mathbf{u}^n(\mathbf{x}_m^n) - \mathbf{u}^n(\mathbf{x}_{m-1}^n)| \leqslant \delta$$

then convergence has been achieved at the current time level and we set $\mathbf{u}^{n+1}(\mathbf{x}) := \mathbf{u}_m^{n+1}(\mathbf{x})$ and proceed to the next time level.

This iterative process converges to zero rapidly—requiring typically two or three iterations for five decimal place accuracy. The scheme lends itself to spectral element discretization where values of $\mathbf{u}(\mathbf{x})$ are easily evaluated away from the nodes. In respect of the last point, the scheme is not compatible with finite difference methods.

Despite the apparent cumbersome nature of the above semi-Lagrangian algorithm, it does have certain advantages over some iterative procedures for treating the convection term, e.g. such as the semi-implicit discretization $\mathbf{u}^n \cdot \nabla \mathbf{u}^{n+1}$. The principal advantage is one of stability since the semi-Lagrangian discretization of the material derivative is performed in the natural direction along particle paths. Another important computational advantage is that, after spatial discretization, the coefficient matrix $\mathbf{M}$ of the resulting system of algebraic equations, $\mathbf{M}\mathbf{x} = \mathbf{b}$, is symmetric and does not change in time since the nonlinear term $\nabla q \cdot \mathbf{T}$ is treated explicitly. Only the right-hand side of this system needs to be updated at every time step. Furthermore, no derivatives of $\mathbf{u}^n$ are required within the semi-Lagrangian step.

We now extend and apply the semi-Lagrangian approach to the treatment of the coupled set of conservation equations. A weak formulation of the governing equations is derived. Defining $\mathbf{u}^n \equiv \mathbf{u}^n(\mathbf{x}^n)$ and $q^n \equiv q^n(\mathbf{x}^n)$, we have the semi-discrete scheme

$$\frac{\mathbf{u} - \mathbf{u}^n}{\Delta t} = \nabla \cdot (-c^2 q \mathbf{I} + \mathbf{T}) + \nabla q \cdot \mathbf{T}$$

$$\frac{q - q^n}{\Delta t} = -\nabla \cdot \mathbf{u}$$

Let Ω denote the region between the journal and bearing. At each time step, a solution is sought in the following spaces:

$$\mathbf{W} = \{\mathbf{w} : w^a \in H^1(\Omega),\ a \in [1, 2],\ \mathbf{w} = \mathbf{V} \text{ on } \Gamma_\mathrm{J},\ \mathbf{w} = \mathbf{0} \text{ on } \Gamma_\mathrm{B}\}$$

$$P = H^1(\Omega)$$

$$\mathbf{R} = [H^1(\Omega)]_s^4$$

where the extra-stress space $\mathbf{R}$ is the space of symmetric 2×2 tensors whose components belong to $H^1(\Omega)$, and Γ_J and Γ_B are the boundaries of the journal and bearing, respectively. We also define the test space, $\mathbf{W}_0$, for the velocity:

$$\mathbf{W}_0 = \{\mathbf{w} : w^a \in H^1(\Omega),\ a \in [1, 2],\ \mathbf{w} = \mathbf{0} \text{ on } \Gamma_\mathrm{J} \text{ and } \Gamma_\mathrm{B}\}$$

DOI: 10.1002/fld

The weak formulation is then: find $\mathbf{u} \in \mathbf{W}$, $q \in P$ and $\mathbf{T} \in \mathbf{R}$, such that

$$\int_\Omega \frac{\mathbf{u} - \mathbf{u}^n}{\Delta t} \cdot \mathbf{w} + \int_\Omega \mathbf{T} : \nabla \mathbf{w} = c^2 \int_\Omega q \, \nabla \cdot \mathbf{w} + \int \nabla q \cdot \mathbf{T} \cdot \mathbf{w}, \quad \forall \mathbf{w} \in \mathbf{W}_0 \tag{29}$$

$$\int_\Omega \left(\frac{q - q^n}{\Delta t} + \nabla \cdot \mathbf{u} \right) p = 0, \quad \forall p \in P \tag{30}$$

$$\int_\Omega \mathbf{T} : \mathbf{W} - \mu \int_\Omega \nabla \mathbf{u} : (\mathbf{W} + \mathbf{W}^{\mathrm{T}}) = v \int_\Omega \nabla \cdot \mathbf{u} \, \mathrm{tr}(\mathbf{W}), \quad \forall \mathbf{W} \in \mathbf{R} \tag{31}$$

5. SPECTRAL ELEMENT DISCRETIZATION

In this paper, the spectral element method is used for the spatial discretization. The spectral element method is based on the weak formulation of the governing equations and possesses advantages of both spectral and finite element methods. The computational domain is partitioned into a number of spectral elements such that the intersections between elements form either a common edge or vertex. The computational efficiency of the method is partly due to the mapping of each spectral element onto the parent element $S = [-1, 1] \times [-1, 1]$ on which the integrals in the weak formulation are evaluated using Gauss–Lobatto Legendre quadrature rules. A typical spectral element mesh for the journal bearing configuration is shown in Figure 4. Let the spectral elements in the radial and azimuthal directions be labelled by $\alpha \in [0, \hat{\alpha}]$ and $\beta \in [0, \hat{\beta}]$, respectively. Then, the Jacobian, $J_{\alpha,\beta}$, of the transformation from a spectral element to the parent element is given by the expression

$$J_{\alpha,\beta}(r, \theta) \equiv \frac{1}{2} \left(\frac{1 - R}{\hat{\alpha} + 1} \right) \left(\frac{\pi}{\hat{\beta} + 1} \right) r(1 - \varepsilon \cos \theta)$$

where

$$r = R + \frac{1}{2} \left(\frac{1 - R}{\hat{\alpha} + 1} \right) (\xi + 2\alpha + 1), \quad \theta = \frac{\pi}{\hat{\beta} + 1} (\zeta + 2\beta + 1) \tag{32}$$

The approximate solution, $\mathbf{u} = [u, v]$ in R^2, is represented as continuous piecewise differentiable polynomials. Each component, u, v, is expressed as a high-order interpolant with respect to the set of Gauss–Lobatto Legendre nodes within each spectral element. Polynomial interpolants of degree N are used in both the radial and angular directions. A 2D grid containing $(N + 1)^2$ points is associated with each element. The velocity representation over the parent element is given by

$$u^a(\xi, \zeta) = \sum_{i=0}^{N} \sum_{j=0}^{N} u_{ij}^a h_i(\xi) h_j(\zeta) \tag{33}$$

DOI: 10.1002/fld

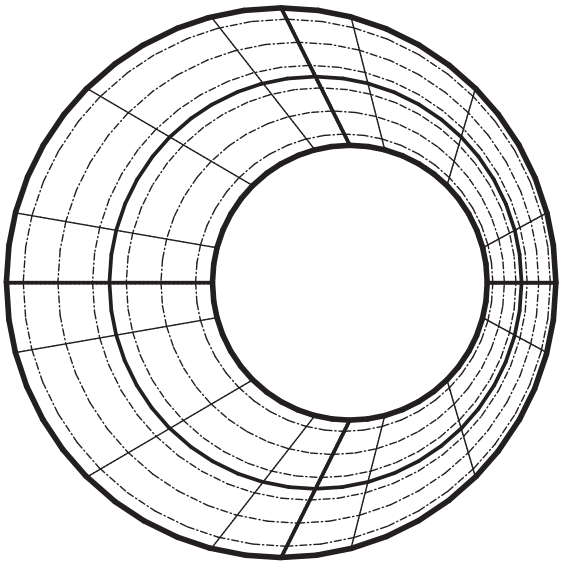

Figure 4. The discretization of the physical domain into four elements in the azimuthal direction and two in the radial direction. The thick lines outline the 4×2 spectral elements and the dashed lines meet at Gauss–Lobatto points for order $N = 4$ in both directions.

where

$$h_i(\xi) \equiv -\frac{(1-\xi^2)L'_N(\xi)}{N(N+1)L_N(\xi_i)(\xi_- \xi_i)} \tag{34}$$

and $L_N(\xi)$ is the Legendre polynomial of degree N. We also approximate the kinematic stress and log density using a basis of the same order:

$$T^{ab}(\xi, \zeta) = \sum_{i=0}^{N} \sum_{j=0}^{N} T_{ij}^{ab} h_i(\xi) h_j(\zeta) \tag{35}$$

$$q(\xi, \zeta) = \sum_{i=0}^{N} \sum_{j=0}^{N} q_{ij} h_i(\xi) h_j(\zeta) \tag{36}$$

In the semi-Lagrangian step of the algorithm, it is necessary to determine $\mathbf{x}^n$ from a knowledge of each Gauss–Lobatto point $\mathbf{x}$ that is uniquely specified by its element (α, β) and its position (i, j) within that element. The next step in the algorithm requires the determination of the element in which $\mathbf{x}^n$ is located. The point $\mathbf{x}^n$ is given in Cartesian coordinates and requires the inverse mapping of (19) to find its corresponding (r, θ) coordinates and thus the element $S_{\alpha,\beta}$ with local coordinates (ξ, ζ). The final step is to calculate the value of $\mathbf{u}^n$ at this point, i.e.

$$\mathbf{u}^n(\mathbf{x}^n) = \sum_{i=0}^{N} \sum_{j=0}^{N} u_{i,j}^n h_i(\xi) h_j(\zeta)$$

DOI: 10.1002/fld

Similarly, the value of q^n is also determined at $\mathbf{x}^n$. This process can generate a position $\mathbf{x}^n$ that lies outside the bearing, particularly if the radii of the journal and bearing are close to one another and the journal is rotating rapidly. For such a simulation, it is reasonable to choose the r coordinate of $\mathbf{x}^n$ to be kept equal to that of $\mathbf{x}$.

The discrete equations are obtained by inserting (33), (35) and (36) into weak formulation (29)–(31), choosing an appropriate test space and approximating the integrals using Gauss–Lobatto Legendre quadrature rules. The following arrays, defined with reference to a local spectral element, are required in order to construct the global system of discrete equations:

$$\bar{A}_{ijkl} \equiv \int_S J(\xi,\zeta) h_i(\xi) h_j(\zeta) h_k(\xi) h_l(\zeta) = J_{ij} \lambda_i \lambda_j \delta_{ki} \delta_{lj} \quad \text{(no sum)}$$

$$\bar{C}_b^{ijkl} \equiv \int_S Z^{cb}(\xi,\zeta) h_i(\xi) h_j(\zeta) [h_k(\xi) h_l(\zeta)]_{,c} = \lambda_i \lambda_j Z_{ij}^{cb} \begin{cases} D_{ik}\delta_{lj}, & c=1 \\ \delta_{ki} D_{jl}, & c=2 \end{cases}$$

$$\bar{f}_a^{kl} \equiv \int_S J(\xi,\zeta) u_a^n \bar{h}_{kl} = J_{ij} \lambda_k \lambda_l u_{akl}^n$$

where J is the Jacobian of the transformation from the spectral element to the parent element, Z^{cb} are the geometric factors associated with the mapping defined by

$$Z_{ij}^{cb} = \left(\frac{\partial \xi^c}{\partial x^b} J \right) (\xi_i, \xi_j) \tag{37}$$

and λ_i, $i = 0, \ldots, N$, are the weights in the Gauss–Lobatto Legendre quadrature rule given by

$$\lambda_i \equiv \int_{-1}^{1} h_i(x)\, \mathrm{d}x = \frac{2}{N(N+1)} \frac{1}{[L_N(\xi_i)]^2}$$

Matrix $\bar{A}$ is the mass matrix. Matrix $D_{ij} = h_j'(\xi_i)$ is the differentiation matrix associated with the interpolants (34) and explicit expressions exist for the entries of D (see, for example, Canuto *et al.* [24]). Note that the entries of these local arrays are defined with respect to a particular spectral element $\Omega^{\alpha,\beta}$ since Z^{cb} and J are element dependent. The unknowns within each element are denoted by q_{ij}, u_{ij}^a and T_{ij}^{ab}. The above system is supplemented with boundary conditions once the global system has been constructed.

The global matrices A^{ijkl}, C_b^{ijkl}, f_a^{kl}, etc. are assembled from the local arrays defined above. Given a local matrix $\bar{L}$ (e.g. $\bar{A}^{ijkl}$, $\bar{C}_b^{ijkl}$, $\bar{f}_a^{kl}$) we construct a global matrix, L, as follows. Define

$$\bar{\bar{L}}_{ijkl}^{\alpha\beta} = \begin{cases} \bar{L}_{ijkl}^{\alpha\beta}, & i,j,k,l \in [0,N] \\ 0 & \text{otherwise} \end{cases}$$

then the global matrix L is given by

$$L_{ijkl} = \sum_{\alpha=0}^{\hat{\alpha}} \sum_{\beta=0}^{\hat{\beta}} \bar{\bar{L}}_{i-\alpha N, j-\beta N, k-\alpha N, l-\beta N}^{\alpha\beta}, \quad i,k \in [0,\hat{N}], \quad j,l \in [0,\hat{M}]$$

DOI: 10.1002/fld

where $\hat{N} = N(\hat{\alpha}+1)$, $\hat{M} = N(\hat{\beta}+1)$. If there is periodicity in the β so that $u^a_{i0}|_{\beta=0} = u^a_{iN}|_{\beta=\hat{\beta}}$ then we modify this expression

$$L_{ijkl} = \sum_{\alpha=0}^{\hat{\alpha}} \left[\sum_{\beta=1}^{\hat{\beta}} \bar{\bar{L}}^{\alpha\beta}_{i-\alpha N, j-\beta N, k-\alpha N, l-\beta N} + \delta^j_{\hat{M}} \bar{\bar{L}}^{\alpha,0}_{i-\alpha N, 0, k-\alpha N, l} \right.$$

$$\left. + \delta^l_{\hat{M}} \bar{\bar{L}}^{\alpha,0}_{i-\alpha N, j-\beta N, k-\alpha N, 0} + \delta^j_{\hat{M}} \delta^l_{\hat{M}} \bar{\bar{L}}^{\alpha,0}_{i-\alpha N, 0, k-\alpha N, 0} \right]$$

where $i, k \in [0, \hat{N}]$, $j, l \in [1, \hat{M}]$. Therefore, in terms of the global arrays, the discretization of (29)–(31), can be written in matrix form

$$\bar{\mathbf{u}} : \bar{\bar{A}} + \Delta t \bar{\mathbf{T}} : \bar{\bar{\mathbf{c}}} = \bar{\mathbf{u}}^n : \bar{\bar{A}} + \Delta t c^2 \bar{q} \cdot \bar{\bar{\mathbf{c}}} + \Delta t \bar{\mathbf{y}} \tag{38}$$

$$\bar{q} \cdot \bar{\bar{A}} + \Delta t \bar{\mathbf{u}} : \bar{\bar{\mathbf{c}}}^{\mathrm{T}} = \bar{q}^n \cdot \bar{\bar{A}} \tag{39}$$

$$\bar{\mathbf{T}} \cdot \bar{\bar{A}} = \mu \bar{\mathbf{u}} : \underline{\bar{\bar{\mathbf{F}}}} + \nu \bar{\mathbf{u}} : \underline{\bar{\bar{\mathbf{G}}}} \tag{40}$$

where the overlines represent the ranks of quantities in the function basis and lowercase (uppercase) bold characters are vectors (matrices) in the physical space and an underlined bold matrix is a third-rank tensor. The single dot product is in the function space and the colon product is on both spaces. The matrix definitions are

$$(\bar{\mathbf{u}})^a_{ij} \equiv u^a_{ij}, \quad (\bar{A})_{ijkl} \equiv A_{ijkl}, \quad (\bar{\mathbf{T}})^{ab}_{ij} \equiv T^{ab}_{ij}, \quad (\bar{\bar{\mathbf{c}}})^b_{ijkl} \equiv C^b_{ijkl}, \quad (\bar{q})_{ij} \equiv q_{ij}$$

$$(\bar{\bar{\mathbf{c}}}^{\mathrm{T}})^a_{ijkl} \equiv C^a_{klij}, \quad (\underline{\bar{\bar{\mathbf{F}}}})^{cab}_{ijkl} \equiv C^b_{klij}\delta^{ac} + C^a_{klij}\delta^{bc}, \quad (\underline{\bar{\bar{\mathbf{G}}}})^{cab}_{ijkl} \equiv C^c_{ijkl}\delta^{ab}$$

$$(\bar{\mathbf{y}})^b_{kl} \equiv \sum_a [(\bar{q} \cdot \bar{\bar{\mathbf{c}}}_T)^a_{kl} T^{ab}_{kl}]$$

The expression for $\bar{\mathbf{y}}$ involves both q and $\mathbf{T}$, and is evaluated explicitly. The unknowns associated with q and $\mathbf{T}$ are eliminated from (38) using (39) and (40), respectively, to obtain the following system for $\bar{\mathbf{u}}$:

$$\bar{\mathbf{u}} : \bar{\bar{\mathbf{M}}} = \bar{\mathbf{v}} \tag{41}$$

where

$$\bar{\bar{\mathbf{M}}} \equiv \bar{\bar{A}} \otimes \mathbf{I} + \{[c^2 \Delta t \bar{\bar{\mathbf{c}}}^{\mathrm{T}} \otimes \mathbf{I} + \mu \underline{\bar{\bar{\mathbf{F}}}} + \nu \underline{\bar{\bar{\mathbf{G}}}}] \cdot \bar{\bar{A}}^{-1} : \bar{\bar{\mathbf{c}}}\} \Delta t \tag{42}$$

and

$$\bar{\mathbf{v}} \equiv \bar{\mathbf{u}}^n : \bar{\bar{A}}\mathbf{I} + c^2 \Delta t \bar{q}^{\,n} \cdot \bar{\bar{\mathbf{c}}} + \Delta t \bar{\mathbf{y}} \tag{43}$$

DOI: 10.1002/fld

Boundary conditions are implemented by modifying (43) so that

$$v_{kl}^b \to v_{kl}^b - \sum_{a=1}^{2} \sum_{j=1}^{\hat{M}} M_{0jkl}^{ab} V_j^a, \quad k \in [1, \hat{N}-1], \quad l \in [1, \hat{M}] \tag{44}$$

where V_j^a are the given values of velocity on the boundary of the journal implied by the no-slip boundary condition with $\hat{M} = N(\hat{\beta}+1)$ and $\hat{N} = N(\hat{\alpha}+1)$.

Once system (41) has been solved for $\bar{\mathbf{u}}$, the pressure and kinematic extra-stress are evaluated using

$$\bar{q} = \bar{q}^n - \Delta t \bar{\mathbf{u}} : \bar{\bar{\mathbf{c}}}^{\mathrm{T}} \cdot \bar{\bar{A}}^{-1} \tag{45}$$

and

$$\bar{\mathbf{T}} = \bar{\mathbf{u}} : [\mu \underline{\bar{\bar{\mathbf{F}}}} + v \underline{\bar{\bar{\mathbf{G}}}}] \cdot \bar{\bar{A}}^{-1} \tag{46}$$

respectively.

On substitution and simplification, we find matrix M_{ijkl}^{ab} reduces to

$$\begin{aligned} \bar{\bar{M}}^{ab} = \bar{\bar{A}}\delta^{ab} + [\mu(\bar{\bar{C}}_T^c \cdot \bar{\bar{A}}^{-1} \cdot \bar{\bar{C}}^c \delta^{ab} + \bar{\bar{C}}_T^b \cdot \bar{\bar{A}}^{-1} \cdot \bar{\bar{C}}^a) \\ + (v + c^2 \Delta t) \bar{\bar{C}}_T^a \cdot \bar{\bar{A}}^{-1} \cdot \bar{\bar{C}}^b] \Delta t \end{aligned} \tag{47}$$

This is a symmetric matrix in the sense that $M_{ijkl}^{ab} = M_{klij}^{ba}$. The log density, in this notation, is given by

$$\bar{q} = \bar{q}^{\,n} - \Delta t \bar{u}^{\,a} \cdot \bar{\bar{C}}_T^a \cdot \bar{\bar{A}}^{-1} \tag{48}$$

Note that this update of q is only required once per time step and not within the iteration scheme.

Once the resulting system of linear equations

$$\bar{\mathbf{u}} : \bar{\bar{\mathbf{M}}} = \bar{\mathbf{v}} \tag{49}$$

has been solved to obtain the global solution $\bar{\mathbf{u}} = \bar{\mathbf{v}} \bar{\bar{\mathbf{M}}}^{-1}$, it remains to determine the solution $u_{ij}^{\alpha\beta,a}$ locally within a spectral element. This may be viewed as the inverse process to that which formed $\mathbf{v}$ from $v_{kl}^{\alpha\beta,b}$. If we define

$$\alpha = \mathrm{int}[(k-1)/N], \quad \beta = \mathrm{int}[(l-1)/N]$$

$$i = (k+\alpha) \bmod (N+1), \quad j = (l+\beta) \bmod (N+1)$$

then

$$u_{ij}^{\alpha\beta,a} = u_{kl}^a, \quad k \in [0, \hat{N}], \quad l \in [1, \hat{M}], \quad a \in [1, 2]$$

where $\hat{N} = N(\hat{\alpha}+1)$, $\hat{M} = N(\hat{\beta}+1)$.

DOI: 10.1002/fld

The values of the solution in real space are given by $u_{ij}^{\alpha\beta,a}$ at the points $(r\cos\theta+\varepsilon(1-r), r\sin\theta)$ where r, θ are given by (32). Thus, each set of values (α, β, i, j) specifies a point at which the values of the three fields $u_{ij}^{\alpha\beta,1}, u_{ij}^{\alpha\beta,2}, q_{ij}^{\alpha\beta}$ are determined.

The force, $\mathbf{F}$, on the journal is given by

$$\mathbf{F} \equiv -\int_C \mathbf{S}\cdot\mathbf{n}\,\mathrm{d}C \tag{50}$$

where C is the boundary of the journal, $\mathbf{n}$ is the unit outward normal to the boundary (radial direction) and $\mathbf{S}$ is the total stress. In two dimensions, this is conveniently written as

$$F^a = \int_C S^{ab}\varepsilon^{bc}\,\mathrm{d}x^c \tag{51}$$

where ε^{bc} is the second-order alternating symbol. In fact, a good approximation to the force in this application is obtained by ignoring the extra stress contribution altogether, since $\mathrm{tr}(\mathbf{S})=0$, and writing the components of force

$$F^a = \int_C S^{ab}\varepsilon^{bc}\,\mathrm{d}x^c \approx \int_C p\varepsilon^{ab}\,\mathrm{d}x^b \tag{52}$$

Using Gaussian quadrature on the journal boundary ($\alpha = i = 0$), this is

$$\begin{aligned}
F^a &= \sum_\beta \int_{-1}^{1} S_{0,j}^{ab}\varepsilon^{bc}\frac{\partial x^c}{\partial\zeta}\,\mathrm{d}\zeta \\
&= \sum_\beta \int_{-1}^{1} \rho_{0,j}(-c^2\delta^{ab}+T_{0,j}^{ab})\varepsilon^{bc}\frac{\partial x^c}{\partial\zeta}\,\mathrm{d}\zeta \\
&= \sum_\beta \int_{-1}^{1} \exp(q_{0,j})(-c^2\delta^{ab}+T_{0,j}^{ab})\varepsilon^{bc}\frac{\partial x^c}{\partial\zeta}\,\mathrm{d}\zeta \\
&= \sum_\beta\sum_j \lambda_j \exp(q_{0,j})(-c^2\delta^{ab}+T_{0,j}^{ab})\varepsilon^{bc}\left.\frac{\partial x^c}{\partial\zeta}\right|_{0,j}, \qquad \beta\in[0,\hat{\beta}],\quad j\in[0,N]
\end{aligned}$$

In practice, we use globally defined quantities so that $j\in[1, N(\beta+1)]$ and

$$F^a = \sum_j \lambda_j \exp(q_{0,j})(-c^2\delta^{ab}+T_{0,j}^{ab})\varepsilon^{bc}\left.\frac{\partial x^c}{\partial\zeta}\right|_{0,j} \tag{53}$$

Similarly, the resultant torque, Λ, on the journal is given by

$$\Lambda = R\int_C S^{ab}n^a\,\mathrm{d}x^b \tag{54}$$

DOI: 10.1002/fld

6. NUMERICAL RESULTS

The numerical results presented in this section are for a journal bearing and lubricant specified by the parameters in the table below. Variations to the values listed here are also considered.

Bearing radius (m)	0.05005
Journal radius (m)	0.05000
Angular velocity (rad/s)	500
Density (kg/m^3)	400
Viscosity (Pa s)	5×10^{-3}

The kinematic viscosity is $\mu \equiv \eta/\rho = 1.25 \times 10^{-5}\,\mathrm{m}^2/\mathrm{s}$. The Reynolds number with dimensionless length based on the average gap is conventionally defined

$$Re = \frac{\omega R_\mathrm{J}(R_\mathrm{B} - R_\mathrm{J})}{\mu}$$

which, for the parameters in the table, gives $Re = 100$. This Reynolds number equates the flow as essentially a channel flow where the width of the channel is taken as a characteristic length and effectively ignores the centripetal forces. On the other hand, it may be argued that a more realistic Reynolds number is $Re = 10^5$ by taking the characteristic length to be that of the radius of the journal, i.e. the ratio of inertial to viscous forces.

The key result of this paper concerns the relationship between the speed of sound c and the force on the journal as it rotates eccentrically within the bearing (see, for example, Figure 5). The extended line joining the journal and bearing centres is defined to be the x-axis. Consider a journal rotating in an anticlockwise direction with relative radii $R = R_\mathrm{J}/R_\mathrm{B} = 0.999$, eccentricity ratio $\varepsilon = 0.98$, kinematic viscosity $\mu = 1.25 \times 10^{-5}\,\mathrm{m}^2/\mathrm{s}$ and angular velocity $\omega = 500\,\mathrm{rad/s}$. In Figure 5 the variation of the force (N) on the journal with respect to the speed of sound is shown. When the speed of sound assumes values in the region of those for water or oil, the component, F_x, of the force on the journal becomes the dominant component and acts in the direction away from the narrow gap. As c increases, the direction of the force on the journal moves towards a position perpendicular to the x-axis in the direction of the fluid flow in the narrow gap (y-axis). Additionally, as the speed of sound increases from $c = 1000\,\mathrm{m/s}$ through $c_\mathrm{oil} = 1500\,\mathrm{m/s}$ to $c = 5000\,\mathrm{m/s}$, the force decreases in magnitude. These values are of theoretical interest only and act as a guide to what to expect when implementing a more realistic equation of state. Also, by means of extrapolation, we estimate that $F_x = 0\,\mathrm{N}$ and $F_y \approx 1000\,\mathrm{N}$ for an incompressible fluid. This implies that an incompressible Newtonian fluid cannot inhibit the journal from making contact with the bearing when the journal is free. This implication agrees with an investigation by Brindley *et al*. [25] who, using lubrication theory, showed that under full-film conditions every journal trajectory spiralled towards the bearing for the range of parameters used in their study. In this situation the load-bearing capacity of the journal is zero and the bearing ultimately fails. However, if the speed of sound is set to almost any reasonable finite value, a component of force in the negative x-direction is introduced. This ensures that the contact between the journal and bearing is avoided.

Figure 5 shows that the magnitude of F_x can exceed that of F_y for sufficiently large eccentricity ratios. This suggests a mechanism whereby cavitation in a lubricant within the journal bearing could have a beneficial effect on its stability through lowering the local speed of sound.

DOI: 10.1002/fld

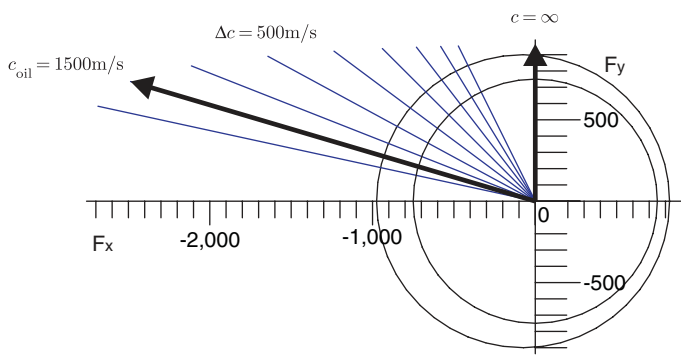

Figure 5. The force (N) on a journal rotating in an anticlockwise direction with relative radii $R = 0.999$, eccentricity ratio $\varepsilon = 0.98$, kinematic viscosity $\mu = 1.25 \times 10^{-5}\,\text{m}^2/\text{s}$ and angular velocity $\omega = 500\,\text{rad/s}$. The radii ($\approx 0.05\,\text{m}$) of the journal and bearing have been exaggerated and superimposed on the forces for clarity.

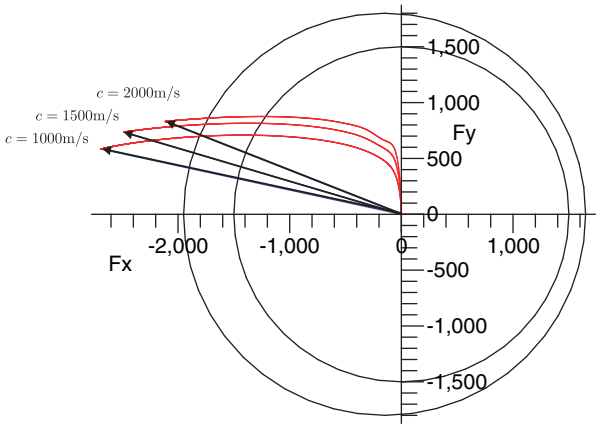

Figure 6. The evolution of the force (N) (grey curved lines) on the journal, towards steady-state vectors with relative radii $R = 0.999$, eccentricity ratio $\varepsilon = 0.98$, kinematic viscosity $\mu = 1.25 \times 10^{-5}\,\text{m}^2/\text{s}$ and angular velocity $\omega = 500\,\text{rad/s}$.

The transient behaviour of the force as the flow approaches steady state is shown in Figures 6 and 7. In Figure 6, the force is shown for values of c between 1000 and 2000 m/s, whereas in Figure 7 the same information is shown for values of c between 2500 and 5000 m/s. The figures show that, at values of c around that of oil, the transient behaviour is smooth, but as the value of c increases F_y exhibits oscillatory behaviour on its way to its steady-state value. Not shown in these figures is the time taken to achieve steady state, which for c_{oil} can be significantly greater than 50 times that of the near incompressible fluids with $c > 3c_{\text{oil}}$.

Figures 8 and 9 are shown for comparison with Figures 6 and 7, but at a smaller eccentricity ratio ($\varepsilon = 0.9$ as opposed to $\varepsilon = 0.98$) revealing the expected smaller forces. These figures also

DOI: 10.1002/fld

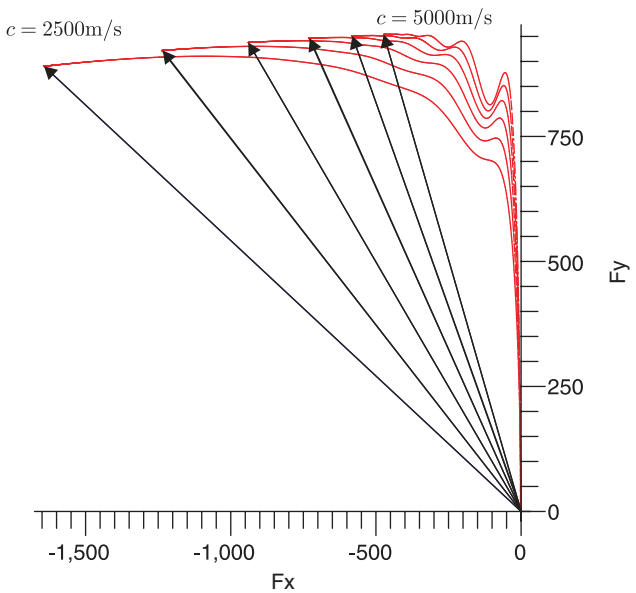

Figure 7. The evolution of the force (N) (grey curved lines) on the journal towards steady state (scaled for clarity) with relative radii $R = 0.999$, eccentricity ratio $\varepsilon = 0.98$, kinematic viscosity $\mu = 1.25 \times 10^{-5}\,\text{m}^2/\text{s}$ and angular velocity $\omega = 500\,\text{rad/s}$. Speed of sound progresses in intervals of 500 m/s from 2500 to 5000 m/s.

show that the magnitude of F_x is relatively smaller than F_y. Figure 9 shows clearly the nature of the oscillations for the higher values of c.

The increasing dominance of F_x over F_y with increasing eccentricity ratio is due entirely to the asymmetry in the pressure distribution around the narrow gap as can be seen in Figure 10. Conversion from log density, q to pressure is done by using $p = c^2\rho = c^2\rho_0 \exp(q)$ so that the pressure difference across the small gap for eccentricity $\varepsilon = 0.9$ is $p \approx 1500^2 \times 400 \times [\exp(0.1) - \exp(-0.08)] = 20\,\text{MPa}$. Eccentricity ratios approaching 0.98 with $(R_\text{B} - R_\text{J})/R_\text{B} = 10^{-3}$ imply a small gap of the order of 1μm and, as such, are only of theoretical interest since, for example, the elasticity of the journal bearing plays a significant part.

The positive peak moves towards $\theta = 0$ as the eccentricity ratio increases causing the resultant force to align more with the negative x-axis (it was this behaviour that instigated the use of stretched spectral elements). The asymmetry about the narrow gap, corresponding to $\theta = 0$ is present for all values of $\varepsilon > 0$ but becomes more marked for $\varepsilon > 0.9$ creating an increasing negative component of the net force on the journal away from the narrow gap.

The torque on the journal is of natural interest to engineers since high torque implies large energy loss and lower efficiency. However, high torque also implies high temperatures increasing the tendency for the fluid to cavitate. Figure 11 shows the transient behaviour of the torque for eccentricity ratios ranging from 0.90 to 0.96. The torque and F_y settle down to steady values long before F_x, as can be seen from this figure since the curves are terminated once F_x achieves its steady-state value. We can also see in this figure that it takes longer to achieve a steady-state value of the torque when the eccentricity ratio is higher.

DOI: 10.1002/fld

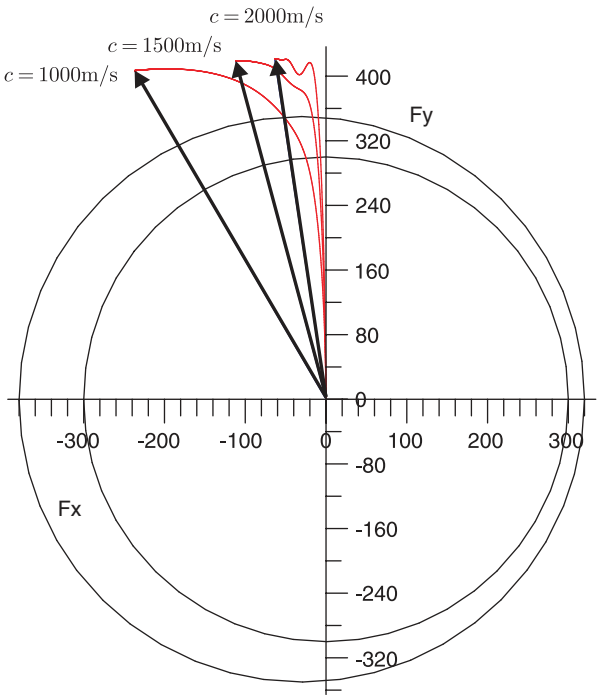

Figure 8. The evolution of the force (N) (grey curved lines) on the journal towards steady state with relative radii $R = 0.999$, eccentricity ratio $\varepsilon = 0.90$, kinematic viscosity $\mu = 1.25 \times 10^{-5}\,\text{m}^2/\text{s}$ and angular velocity $\omega = 500\,\text{rad/s}$.

The driving force behind the net torque is the shear stress around the journal. This is shown in Figure 12, revealing again an asymmetry about the narrow gap $\theta = 0$. For $\varepsilon > 0.5$, the shear stress becomes negative in a region around the narrow gap. This latter feature remains the case for a near incompressible fluid characterized by large sound speed, c.

Figure 13 is similar to Figure 10 except that the pressure curves are generated by changing the speed of sound (rather than changing the eccentricity ratio) from 1000 to 5000 m/s in increments of 500 m/s. For smaller values of c, pressure curves are generated that are almost symmetric about the narrow gap at $\theta = 0$. Figure 14 shows density curves, generated by changing angular velocity, ω. The behaviour suggests that the force on the journal is roughly linear in response to changes in ω within this parameter range.

Finally, the effect of changing the bulk viscosity on the behaviour of the journal is shown in Figure 15 by plotting $\ln \rho$ (left) and $\rho - S_{rr}/c^2$ (right) around the surface of the journal. This figure shows categorically that the effects of bulk viscosity are absolutely negligible and therefore its value can be chosen conveniently (though the choice must be positive so as not to violate the second law of thermodynamics). The natural candidate is for vanishing bulk viscosity (implying, $\nu = -2\mu/3$), but a choice of, for example, $2\mu/3$ (implying $\nu = 0$) may also be convenient. The figure also demonstrates that, even at the large bulk viscosities considered, the pressure at the surface of the journal given by the normal stress (as opposed to p), is negligible.

DOI: 10.1002/fld

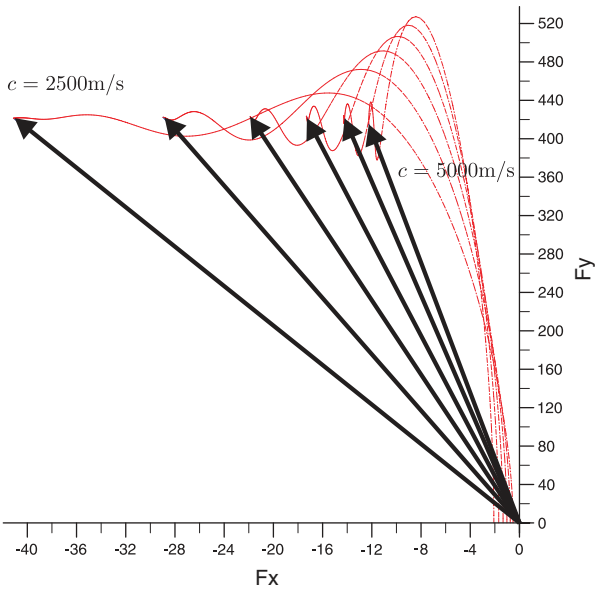

Figure 9. The evolution of the force (N) (grey curved lines) on the journal towards steady state (scaled for clarity) with relative radii $R = 0.999$, eccentricity ratio $\varepsilon = 0.90$, kinematic viscosity $\mu = 1.25 \times 10^{-5}\,\mathrm{m}^2/\mathrm{s}$ and angular velocity $\omega = 500\,\mathrm{rad/s}$. Speed of sound progresses in intervals of 500 m/s from 2500 to 5000 m/s.

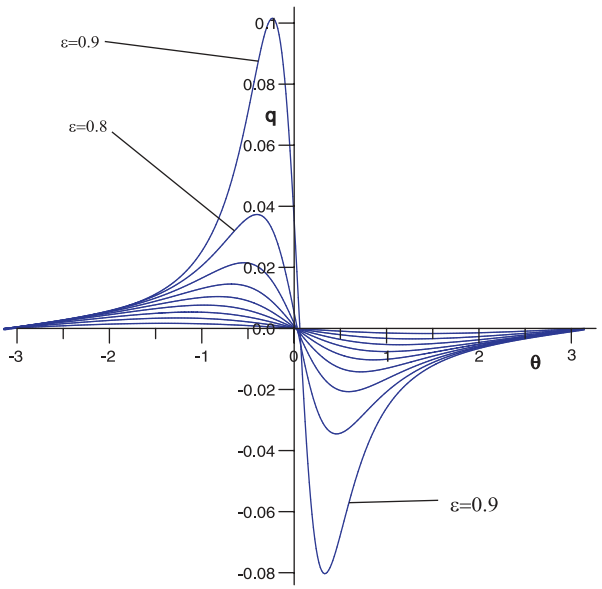

Figure 10. Profiles of $\ln \rho$ as a function of θ on the surface of the journal for different eccentricity ratios ($\varepsilon = 0.1$–0.9 in steps of 0.1) with $c = 1500\,\mathrm{m/s}$, $\mu = 1.25 \times 10^{-5}\,\mathrm{m}^2/\mathrm{s}$, $\omega = 500\,\mathrm{rad/s}$ and $R = 0.999$.

DOI: 10.1002/fld

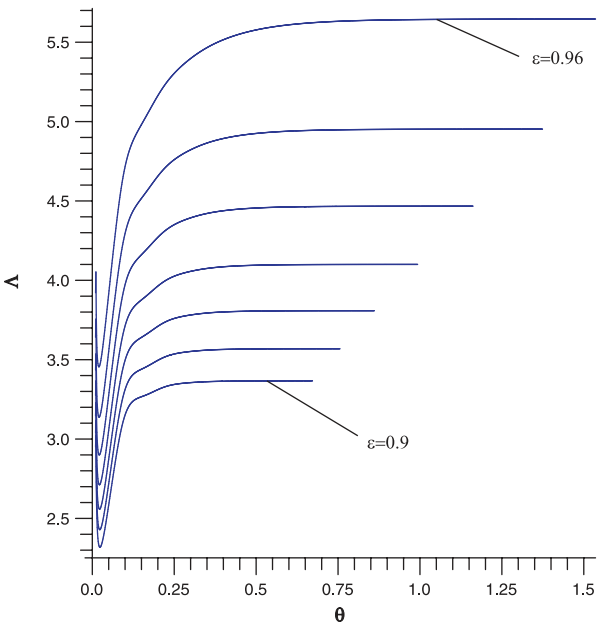

Figure 11. The evolution of the torque (N m) on the journal towards steady state for $0.90 \leqslant \varepsilon \leqslant 0.96$ with relative radii $R = 0.999$, kinematic viscosity $\mu = 1.25 \times 10^{-5}\,\mathrm{m}^2/\mathrm{s}$, speed of sound $c = 1500\,\mathrm{m/s}$ and angular velocity $\omega = 500\,\mathrm{rad/s}$.

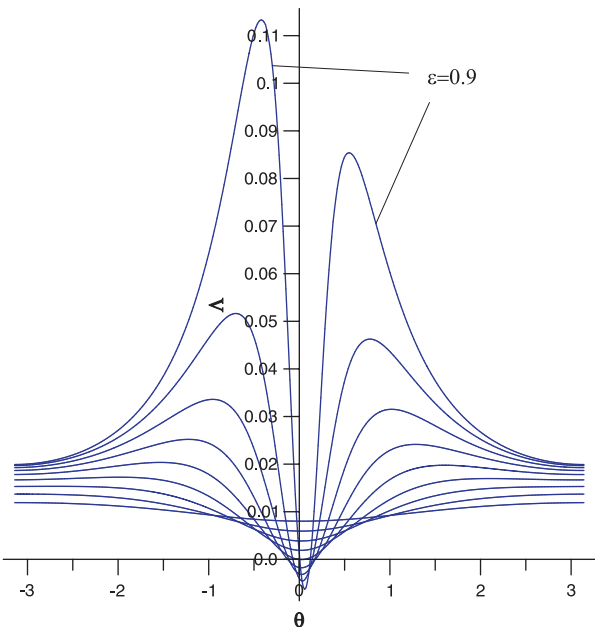

Figure 12. The shear stress $S_{r,\theta}$ (Pa) on the journal for $0.1 \leqslant \varepsilon \leqslant 0.9$ and $c = 1500\,\mathrm{m/s}$ revealing again an asymmetry about the narrow gap.

DOI: 10.1002/fld

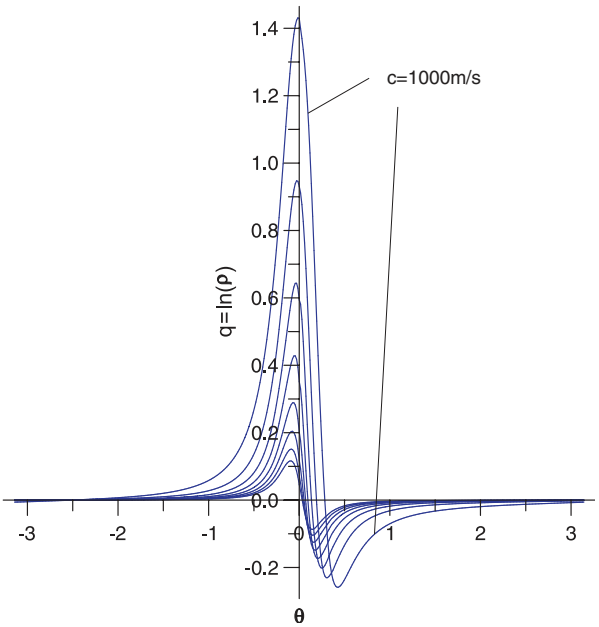

Figure 13. Profiles of $q = \ln \rho$ as a function of θ on the surface of the journal for a fixed eccentricity ratio $\varepsilon = 0.98$. The figure shows the effect of varying the speed of sound from $c = 1000$ to $5000\,\mathrm{m/s}$. The smaller the value of c the larger the values of ρ and the peak moves towards the narrow gap, showing that decreased c increases the component of force away from the narrow gap.

6.1. Discussion on numerical convergence and computing time

The spectral element method allows for mesh refinement either by increasing the number of elements or through increasing the order of polynomial approximation. Thus, we have two independent methods for checking the accuracy of our numerical predictions. This is obviously very satisfactory when both methods of refinement agree. In Table II, it can be seen that increasing the number of elements beyond 16 has little effect on the value of the cosine of the force direction, $F_x/|\mathbf{F}|$, and the approximation has effectively converged. In Table I, the effect of changing the order of polynomial approximation for a fixed number of elements on the cosine of the force direction is shown. Since the agreement between successive entries in this table is $\sim 0.01\%$, this provides confidence in the convergence of the approximation with mesh refinement.

Table III shows the computing times for different values of $\hat{\beta} + 1$ for polynomial order $N = 6$ and just one spectral element in the radial direction. The matrix dimension is $2(N(\hat{\alpha}+1)-1)N(\hat{\beta}+1) = 60(\hat{\beta}+1)$, e.g. for $\hat{\beta} + 1 = 8$ gives a 480×480 matrix. Note, that this slightly complicated formula for the matrix dimension comes about because of the periodicity at one of the boundaries and the coincidence of spectral elements at each element boundary. For this linear model, the matrix is only set up once. Refinements, say shear thinning, involves some setting up of the matrix at each time step with consequent increased run times.

DOI: 10.1002/fld

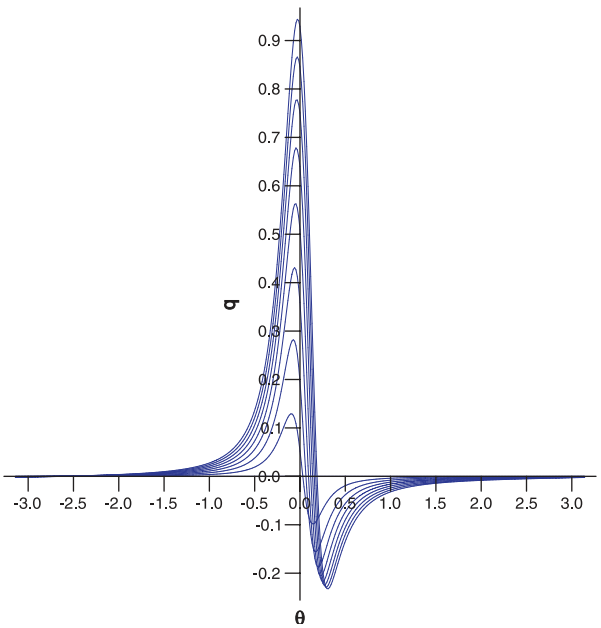

Figure 14. Profiles of $q = \ln \rho$ as a function of θ on the surface of the journal for a fixed eccentricity ratio of $\varepsilon = 0.98$. The figure shows the effect of varying the angular velocity uniformly from 0 to 500 rad/s with $\varepsilon = 0.98$, $R = 0.999$, $c = 1500\,\mathrm{m/s}$ and $\mu = 1.25 \times 10^{-5}\,\mathrm{m^2/s}$.

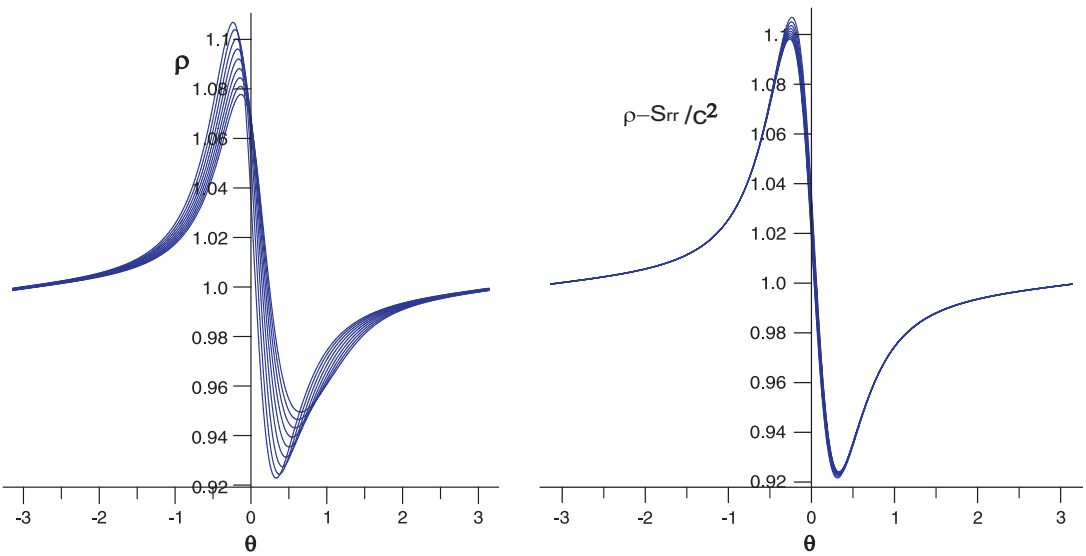

Figure 15. Profiles of $q = \ln \rho$ (left) and $\rho - S_{rr}/c^2$ (right) as a function of θ on the surface of the journal, as the kinematic bulk viscosity $\frac{2}{3}\mu + \nu$ goes from zero to 100 K Pa s (a very large value compared with μ). The other parameters used are $c = 1500\,\mathrm{m/s}$, $\mu = 1.25 \times 10^{-5}\,\mathrm{m^2/s}$, $\varepsilon = 0.9$, $R_\mathrm{J} = 0.999$ and $\omega = 500\,\mathrm{rad/s}$.

DOI: 10.1002/fld

Table I. The values of $F_x/|\mathbf{F}|$ as a function of ε for different orders of polynomial approximation with 16 spectral elements ($\hat{\alpha}=15$), $c=1250\,\mathrm{m/s}$, $\mu=1.25\times10^{-5}\,\mathrm{m^2/s}$, $R=0.999$.

	Polynomial order N			
ε	6	7	8	9
0.80	−0.1174	−0.1176	−0.1176	−0.1176
0.82	−0.1392	−0.1393	−0.1393	−0.1393
0.84	−0.1685	−0.1686	−0.1686	−0.1686
0.86	−0.2092	−0.2093	−0.2094	−0.2094
0.88	−0.2680	−0.2681	−0.2682	−0.2682
0.90	−0.3558	−0.3558	−0.3560	−0.3561
0.92	−0.4883	−0.4880	−0.4884	−0.4886
0.94	−0.6738	−0.6727	−0.6733	−0.6737
0.96	−0.8640	−0.8624	−0.8635	−0.8640
0.98	−0.9689	−0.9687	−0.9699	−0.9699

Note: The results suggest that for $N=9$ the values have converged to $\sim 0.01\%$.

Table II. The values of $F_x/|\mathbf{F}|$ as a function of ε for different numbers of spectral elements with $N=6$, $c=1250\,\mathrm{m/s}$, $\mu=1.25\times10^{-5}\,\mathrm{m^2/s}$, $R=0.999$.

	Number of spectral elements $\hat{\beta}+1$			
ε	8	16	32	64
0.80	−0.1172	−0.1174	−0.1175	−0.1175
0.82	−0.1390	−0.1391	−0.1392	−0.1392
0.84	−0.1685	−0.1685	−0.1685	−0.1685
0.86	−0.2098	−0.2092	−0.2093	−0.2093
0.88	−0.2700	−0.2680	−0.2681	−0.2681
0.90	−0.3605	−0.3558	−0.3560	−0.3560
0.92	−0.4974	−0.4883	−0.4887	−0.4887
0.94	−0.6867	−0.6738	−0.6741	−0.6741
0.96	−0.8795	−0.8640	−0.8643	−0.8644
0.98	−0.9862	−0.9689	−0.9700	−0.9700

Note: The results suggest that convergence to $\sim 0.01\%$ is satisfied for 32 elements and also in good agreement with the higher-order result given in Table I.

Table III. The set-up time and total computing time to achieve steady state after 100 time steps for different refinements of $\hat{\beta}$ with $N=6$, $\alpha=0$.

	Number of spectral elements $\hat{\beta}+1$				
Time (s)	8	10	12	14	16
Set-up	30.0	60.5	107.0	171.1	255.1
Total	68.6	114.9	178.9	262.1	369.7

Note: We note that over 64% of the total computing time is due to the initial setting up of the matrix and increases with the number of elements.

DOI: 10.1002/fld

7. CONCLUSIONS

The main result in this paper is the important role played by compressibility in enhancing the load-bearing capacity of a journal bearing. For a journal bearing of radius 0.05 m rotating at 500 rad/s, the speed of the fluid in the gap is of the order of 1/50 of that of the speed of sound in the fluid, i.e. the Mach number is 0.02. For such a low Mach number, one might reasonably expect the effects of compressibility to be negligible. However, in the case of a journal bearing, a Newtonian fluid generates an (almost) antisymmetric pressure field about the small gap. Any mechanism which breaks this antisymmetry will generate a resultant force in the direction of the line joining the two centres (indeed a pressure thinning mechanism, as used here, can also do this). However, it is the compressibility of the fluid that plays the most significant role. The effect being amplified by high eccentricity which squeezes the fluid at the small gap. For $\varepsilon = 0.98$, $R = 0.999$, the ratio of large to small gap is approximately 100:1.

An advantageous feature of the model used here is its similarity to constant density (incompressible) Navier–Stokes equations, due largely to a linear equation of state $p = c^2\rho$ and the use of the parameter $q \equiv \ln \rho$, which together with the semi-Lagrangian discretization of the material derivatives ensures that many of the terms in the equations remain linear and allows a very efficient spectral element numerical scheme.

The compressible model described in this paper is currently being extended to include further developments in the modelling of lubricating oils such as cavitation. This model will feature a temperature-dependent vaporization point below which compressibility effects will be prominent due to lower values of the sound speed. The other natural development in the near future is to examine the dynamics of a journal bearing, under an external applied load, of a free journal under the present model and an extension of the model to include viscoelasticity.

REFERENCES

1. Tower B. Second report on friction experiments (experiments on the oil pressure in a bearing). *Proceedings of the Institution of Mechanical Engineers* 1885; 58–70.
2. Petrov NP. Friction in machines and the effect of the lubricant. *Inzhenerno Zhurnal St. Petersburg* 1883; **1**:71–140.
3. Petrov NP. Friction in machines and the effect of the lubricant. *Inzhenerno Zhurnal St. Petersburg* 1883; **2**:227–279.
4. Petrov NP. Friction in machines and the effect of the lubricant. *Inzhenerno Zhurnal St. Petersburg* 1883; **3**:377–436.
5. Petrov NP. Friction in machines and the effect of the lubricant. *Inzhenerno Zhurnal St. Petersburg* 1883; **4**:535–564.
6. Reynolds O. On the theory of lubrication and its application to Mr. Beauchamp Tower's experiments. *Philosophical Transactions of the Royal Society* 1886; **177**:157–234.
7. Hamrock BJ. *Fundamentals of Fluid Film Lubrication*. McGraw-Hill: New York, 1994.
8. Gwynllyw DRh, Davies AR, Phillips TN. A moving spectral element approach to the dynamically loaded journal bearing problem. *Journal of Computational Physics* 1996; **123**:476–494.
9. Gwynllyw DRh, Davies AR, Phillips TN. On the effects of a piezoviscous lubricant on the dynamics of a journal bearing. *Journal of Rheology* 1996; **40**:1239–1266.
10. Gwynllyw DRh, Phillips TN. Preconditioned iterative methods for unsteady non-Newtonian flow between eccentrically rotating cylinders. *SIAM Journal on Scientific Computing* 1996; **17**:1369–1394.
11. Phillips TN, Need RE, Davies AR, Williamson B, Scales LE. The effect of viscoelasticity on the performance of dynamically loaded journal bearings. *Technical Report 982639*, Society of Automotive Engineers, 1998.
12. Belblidia F, Keshtiban IJ, Webster MF. Stabilised computations for viscoelastic flows under compressible implementations. *Journal of Non-Newtonian Fluid Mechanics* 2006; **134**:56–76.

DOI: 10.1002/fld

13. Gwynllyw DRh, Phillips TN. Some issues regarding spectral element meshes for moving journal bearing systems. *International Journal for Numerical Methods in Fluids* 2005; **48**:423–454.
14. Barus C. Isothermal, isopiestics and isometrics to viscosity. *American Journal of Science* 1893; **45**:87–96.
15. Dowson D, Higginson GR. *Elastohydrodynamic Lubrication—the Fundamentals of Roller and Gear Lubrication.* Pergamon Press: Oxford, U.K., 1966.
16. Gad el Hak M. Questions in fluid mechanics: Stoke's hypothesis for a Newtonian, isotropic fluid. *Journal of Fluids Engineering* 1995; **117**:3–5.
17. Phan-Thien N. *Understanding Viscoelasticity*. Springer: Berlin, 2002.
18. Kirkwood JG, Bethe H. The pressure wave produced by an underwater explosion. Part I. *Technical Report 588*, 1942.
19. Kirkwood JG, Bethe H. The pressure wave produced by an underwater explosion. Part III. *Technical Report 813*, 1942.
20. Houpert LG. New results of traction force calculations in elastohydrodynamic contacts. *Journal of Tribology-Transactions of the ASME* 1985; **107**:241–248.
21. Billingham J, King AC. *Wave Motion*. Cambridge Texts in Applied Mathematics. Cambridge University Press: Cambridge, U.K., 2001.
22. Karniadakis GE, Israeli M, Orszag SA. High-order splitting methods for the incompressible Navier–Stokes equations. *Journal of Computational Physics* 1993; **97**:414–443.
23. Deville MO, Fischer PF, Mund EH. *High-order Methods for Incompressible Fluid Flow*. Cambridge University Press: Cambridge, U.K., 2002.
24. Canuto C, Hussaini MY, Quarteroni A, Zang TA. *Spectral Methods in Fluid Dynamics*. Springer: Berlin, 1988.
25. Brindley J, Elliott L, McKay JT. The role of cavitation in whirl instability in a rotor bearing. Part 1: The π-film model. *Journal of Applied Mechanics* (ASME) 1983; **50**:877–885.

DOI: 10.1002/fld